*Clays and Clay Minerals*, Vol. 49, No. 4, 277–285, 2001.

# THICKNESS AND SURFACE CHARACTERISTICS OF COLLOIDAL 2:1 ALUMINOSILICATES USING AN INDIRECT FOURIER TRANSFORM OF SMALL-ANGLE X-RAY SCATTERING DATA

CHAO SHANG[1], JAMES A. RICE[1], AND JAR-SHYONG LIN[2]

[1]Department of Chemistry and Biochemistry, South Dakota State University, Brookings, South Dakota 57007, USA
[2]Solid State Division, Oak Ridge National Laboratory, Oak Ridge, Tennessee 37831, USA

**Abstract**—An indirect Fourier transformation applied to small-angle X-ray scattering data has been used to determine the thickness and surface properties of two common clay minerals. For an illite system, the particle density distribution function (PDDF) generated by the analysis gave a correct description of particle geometry, and the calculated electron density profile was in accordance with the theoretical electron density distribution for this mineral. This approach provides the opportunity to determine the thickness of fundamental particles of illite while avoiding the difficulties encountered in other methods. Both the PDDF and the electron density profile accurately predict the thickness of Na-montmorillonite layers, and the results suggest that an electron inhomogeneity exists at the interface of this mineral.

**Key Words**—Illite, Indirect Fourier Transform, Montmorillonite, SAXS, Thickness.

## INTRODUCTION

Small-angle X-ray scattering (SAXS) is a technique widely used to determine the internal and external structure of colloidal particles over a wide range of length scales (Guinier and Fournet, 1955; Schmidt, 1995). Synthetic and natural clay minerals form colloidal suspensions that are ideal for model testing and studying colloidal behaviors such as swelling, interparticle forces and structural organization (van Olphen, 1963). These studies have both theoretical and industrial significance. The thickness, interparticle spacing in hydrated states, and the influence of interparticle forces fall into the characterization length scale of SAXS and have been investigated by this method in the past (Hight *et al.*, 1960, 1962; Taylor and Schmidt, 1969; Morvan *et al.*, 1994; Pignon *et al.*, 1997; Saunders *et al.*, 1999).

In previous studies (*e.g.* Hight *et al.*, 1960; Saunders *et al.*, 1999), well-characterized smectites were used in thickness determinations with the SAXS method based on an assumed particle shape. This approach has limited application in the determination of thickness of natural clay minerals which often do not have the required regular dimension in at least two coordinates. Hight *et al.* (1960) also employed the absolute scattering intensity at zero angle to derive the thickness of montmorillonite, but the method was subject to large experimental errors. Furthermore, the spacing and layer thickness of expandable clays can be measured conveniently by X-ray diffraction (XRD).

Illites are a group of non-expandable and micaceous minerals, often present in nature as mixed-layer components with varying proportions of illite-smectite (I-S) layers. This interstratification makes it difficult to determine the thickness of the fundamental illite particle by conventional analysis of X-ray data. Various attempts have been made in recent years using TEM, fixed cation content, and X-ray peak broadening (Nadeau *et al.*, 1984; Środoń *et al.*, 1990, 1992; Drits *et al.*, 1997, 1998). Each of these methods suffers from its own uncertainties. As noted by Drits *et al.* (1997, 1998), the thickness of most illite samples present in nature can be measured by SAXS, and this method offers two advantages over other methods: illite particles in dilute suspensions are independent and free of swelling problems, and at least one million particles are scanned and averaged. By comparison, TEM only 'sees' hundreds of particles.

Glatter (1977, 1980) developed a numerical method utilizing an indirect Fourier transform (IFT) to calculate the PDDF that describes the averaged geometry of all scattering particles. Using this method, it is possible to calculate particle thickness without making any assumptions about particle shape. The IFT minimizes the termination effects encountered when data are converted from reciprocal space to real space with a direct Fourier transformation (Guinier and Fournet, 1955; Hight *et al.*, 1962). Furthermore, deconvolution of the PDDF gives the electron density distribution for central symmetric scatterers (Glatter, 1982) that reveals their internal structure.

Here we report the use of SAXS and the indirect Fourier transform to determine the thickness of the Silver Hill illite and a montmorillonite (Wyoming bentonite) sample. Use of montmorillonite serves to verify the numerical method and provides evidence of surface inhomogeneity related to surface charge density.

## THEORY

For a thin-layer particle such as a 2:1 aluminosilicate with two dimensions ($D$) far larger than the thick-

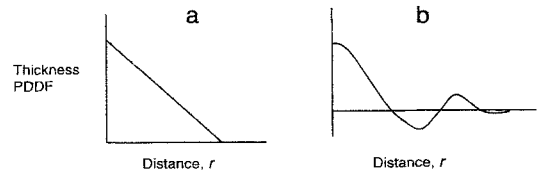


Figure 1. Schematic representations of the PDDF, $P_t(r)$, of lamellae with homogeneous (a) and inhomogeneous (bilayer) (b) electron distributions.

ness ($T$), the scattering intensity can be expressed as a cosine-Fourier transform of the pair distance distribution function ($P_t(r)$) of the particle thickness (Glatter, 1982; Porod, 1982; Glatter *et al.*, 1996):

$$I(q) = 2\pi A I_t(q)/q^2$$

$$= 4\pi A \int_0^\infty (1/q^2) P_t(r)\cos(qr)\, dr \quad \text{or} \quad (1)$$

$$I_t(q) = I(q)q^2/2\pi A$$

$$= 2 \int_0^\infty (1/q^2) P_t(r)\cos(qr)\, dr \quad (2)$$

where: $I_t(q)$ is the particle cross-section scattering intensity; $q$ is the scattering vector which is related to the scattering angle, $\theta$, and a given wavelength, $\lambda$, by:

$$q = (4\pi/\lambda)\sin(\theta/2); \quad (3)$$

$A$ is the cross-section area, and $r$ is the distance between any two points on a particle. The inverse transformation of equation 2 gives:

$$P_t(r) = 1/\pi \int_0^\infty I_t(q)\cos(qr)\, dr \quad (4)$$

The scattering length density profile, or the electron density contrast, $\rho_t(r)$, between the medium and scattering particle can also be calculated by the cosine transformation:

$$\rho_t(r) = 1/\pi \int_0^\infty (I_t(q))^{1/2}\cos(qr)\, dr \quad (5)$$

because the electron density of a silicate layer can be assumed to be homogeneous across the two large dimensions with variation only along the third dimension, and it is centrosymmetric (Glatter, 1982). Determination of $\rho_t(r)$ from equation 5 suffers from phase problems, and in practice $\rho_t(r)$ is calculated from the PDDF by a convolution square root technique (Glatter, 1982) for thin particles by equation 6:

$$P_t(r) = \rho_t(x)^*\rho_t(-x) \quad (6)$$

where * indicates a convolution operation, and $x$ is the spatial coordinate of the third dimension.

Since $P_t(r) = 0$ and $\rho_t(r) = 0$ at $r \geq T$ (*i.e.* the thickness of the clay layer), both functions reveal the layer thickness. The scattering length density, $\rho_t$, represents the electron density difference between the silicate layer and the solvent. Thus the scattering density profile $\rho_t(r)$ allows the estimation of the electron homogeneity of the clay layer along the third dimension or the surface roughness of clay. Figure 1 shows the typical PDDF curves for lamellae with different electron distributions.

The clay particle layer thickness can also be derived from the Guinier approximation when $q$ is small (Guinier and Fournet, 1955):

$$I_t(q) = I(q)q^2/2\pi A = (\rho_t)^2 T^2 \exp(-q^2 R_t^2), \quad (7)$$

where $R_t$ is the radius of gyration for the thickness, $R_t^2$ is the negative of the slope of a ln $I_t$ ($q$) *vs.* $q^2$ plot, and $R_t^2 = T^2/12$. Equation 7 also serves as a guideline for SAXS data analysis since it indicates that the particles studied have a laminar shape if the plot of ln ($I(q)$ $q^2$) *vs.* $q^2$ is linear as $q \to 0$.

## DATA ANALYSIS

With the IFT method (Glatter, 1995), the PDDF is approximated by a linear combination

$$P_t(r) = \sum_{\nu=1}^{N} C_\nu \varphi_\nu(r) \quad (8)$$

where $\varphi_\nu$ ($r$) are basis functions chosen as cubic B-splines, $N$ is the number of functions, and $C_\nu$ are expansion coefficients. Another linear expansion is used to approximate the scattering intensity

$$I(q) = \sum_{\nu=1}^{N} C_\nu \Psi_\nu(q) \quad (9)$$

Combining 1, 8 and 9 with the boundary $P_t(r) \neq 0$, $r_{min} \leq r \leq r_{max}$, $\Psi_\nu$ ($q$) is related to $\varphi_\nu(r)$ through

$$\Psi_\nu(q) = 4\pi \int_{r_{min}}^{r_{max}} \varphi_\nu(r)\cos(qr)\, dr \quad (10)$$

The coefficient $C_\nu$ can be determined by minimizing

$$\text{min.} = (L + \lambda N_c) \quad (11)$$

with

$$L = \sum_{\nu=1}^{N} \left[I(q) - \sum C_\nu \Psi_\nu(q)\right]^2 / \delta^2(q) \quad (12)$$

and

$$N_c = \sum_{\nu=1}^{N} (C_{\nu+1} - C_\nu)^2 \quad (13)$$

The purpose of $N_c$ is to minimize any artificial oscillation in the PDDF. The overall minimization is achieved by determining an optimum value of $\lambda$, the Lagrange multiplier, by the inflection-point method, *i.e.* $\lambda_{opt}$ exists where the second derivative of $N_c$ changes sign and its first derivative is at the minimum. Correction for slit smearing is unnecessary in this study

https://doi.org/10.1346/CCMN.2001.0490401 Published online by Cambridge University Press

because the SAXS camera uses point collimation; however, the correction can be carried out in a fashion similar to that described above. The IFT procedure can be accomplished with a Fortran computer program developed by Glatter (1977), and released as 'ITP'.

## EXPERIMENTAL

### *Clay samples*

Montmorillonite (SWy-2) and illite (IMt-2) samples were obtained from the Source Clay Minerals Repository, University of Missouri–Columbia, Missouri. The minerals are well-characterized (Hower and Mowatt, 1966; van Olphen and Fripiat, 1979). We followed the pretreatment procedure described by Rich and Barnhisel (1977). In brief, 25 g of clay sample were placed in a 500 mL Erlenmeyer flask, and then 250 mL of pH 5 acetate buffer were added to remove carbonates. The mixture was heated in a water bath (90°C) for 2 h before being centrifuged to discard the supernatant. Hydrogen peroxide (30%) was added to the clay samples to oxidize organic matter, and the sample was digested for 12 h at 90°C in a water bath. After organic matter oxidation, the sample was suspended in citric-bicarbonate buffer (pH 8.3) at 80°C and an appropriate amount of dithionite powder was added to remove free iron oxides. Finally, the sample was transferred into a 1 L plastic bottle and the clay was shaken with 1 M NaCl for 6 h before centrifugation to discard the supernatant. The salt washing was repeated once. The Na-saturated clay was washed once with distilled and deionized water and dialyzed against water until it was free of chloride (silver nitrate test).

The <0.08 μm Na-montmorillonite fraction and <0.1 μm illite fraction were obtained by centrifugation (IEC CRU-5000). Dilute clay fraction suspensions were concentrated on a rotary evaporator to produce concentrated clay stocks (3% for montmorillonite and 10% for illite). The exact clay concentrations were determined by oven drying a known volume or weight of clay suspension at 110°C and weighing.

### *SAXS measurement*

The SAXS measurements were performed with the 10 m SAXS camera at Oak Ridge National Laboratory, Oak Ridge, Tennessee. The camera utilizes point collimation to eliminate slit effects in conjunction with a two-dimensional position sensitive detector. It is described in detail by Wignall *et al.* (1990). The sample-to-detector distance was 1.119 m for large-angle region measurements ($q$ = 0.18–4.5 $nm^{-1}$) and 5.119 m for the low-angle region ($q$ = 0.053–0.9 $nm^{-1}$). Cu Kα radiation (λ = 0.154 nm) with a power setting at 40 kV and 60 mA was used. The detector sensitivity was calibrated with a Fe-55 standard. The transmission coefficient was determined for each sample and used to correct scattering data to absolute intensities.

The clay sample concentrations ranged from 0.5 to 5% (w/w) for montmorillonite and 0.5 to 20% (w/w) for illite. Clay suspensions were mounted in a metal SAXS cell fitted with a Kapton window and having a 1 cm internal diameter and 1-mm thickness. The data acquisition time varied from 30 to 180 min depending on sample concentration and the scattering vector range. The background scattering of a sample blank was subtracted from each sample before further data analysis for the montmorillonite systems. For illite samples, the slope of the Porod plot ($I_{exp}$ $q^4$ *vs.* $q^4$) was used for background subtraction.

## RESULTS AND DISCUSSION

The variation in scattering intensity (normalized for clay concentration) as a function of $q$ for various clay concentrations is shown in Figure 2. All the scattering curves overlap at large $q$ but some deviate at low q. For illite samples (Figure 2a), the scattering curves of 1%, 2% and 3% are almost identical over the entire $q$ range but large deviations are found for higher concentrations over the innermost $q$ region indicating the presence of interparticle or concentration effects (Pilz, 1982) when the clay concentration is >3%. There are apparently large experimental errors associated with the 0.5% clay curve, which deviates from the dilute sample group. This is attributed to low scattering intensity at low $q$ values. Therefore, the scattering curves in the 1–3% concentration range are equally representative of this mineral's scattering properties. The concentration effect is much more pronounced in montmorillonite systems, being observable even at a 1% clay concentration (Figure 2b). There is a broad hump on the 3% and 5% curves between $q$ = 0.1 and 0.2 $nm^{-1}$ which is usually believed to account for the structure factor maximum of a scattering system (Morvan *et al.,* 1994). To show the concentration effect, the scattering curves of 0.5%, 1% and 2% were extrapolated to zero concentration by a linear Zimm plot. It is clear from this plot that all systems are affected by interparticle interactions (*i.e.* deviations from the extrapolated curve). Although this is expected because of the positive charges on the edge of montmorillonite layers causing edge-surface interaction (van Olphen, 1963), it is still of interest that the effect is confirmed by SAXS through the comparison of two contrasting minerals.

Usually when the geometry of particles studied is not known *a priori,* a general PDDF is calculated to indicate the particle's shape before a specific PDDF is obtained for that type of particle (Glatter, 1991; Strey *et al.,* 1996; Iampietro *et al.,* 1998). In this study, the general PDDF does not reveal the true maximum dimensions of the clay particles since their long dimension may reach 80 nm or greater, which is beyond the limit of this SAXS instrument, although the calculated PDDFs (data not shown) did resemble the documented

https://doi.org/10.1346/CCMN.2001.0490401 Published online by Cambridge University Press

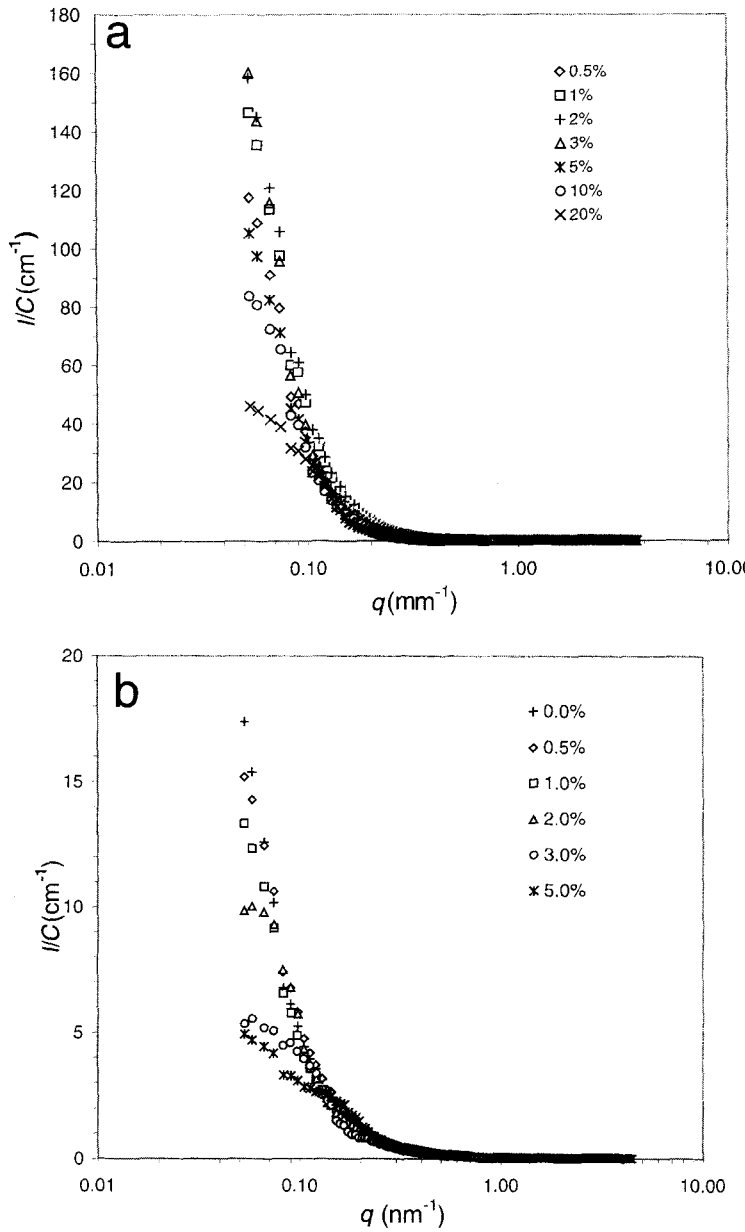


Figure 2. Scattering curves for illite (a) and montmorillonite (b) suspensions of various particle concentrations. The experimental scattering intensity was first subtracted from the background scattering which was then divided by the clay concentration (mg $mL^{-1}$) (see text for more details). "0.0%" represents the extrapolated curve at zero particle concentration.

PDDF for lamellae (Glatter, 1982). Therefore, our treatment has focused on the thickness PDDF and scattering length density profiles since layer silicates are known to be lamellae in dispersion. To avoid any possible interparticle interaction effects, Müller and Glatter (1982) recommended that either the extrapolated zero concentration curve or the most dilute curve with the innermost portion of curve truncated should be used for calculating the PDDF. Based on the results shown in Figure 2, we used the latter approach with the 2% curve of illite and the cut-off 0.5% curve of montmorillonite in subsequent PDDF calculations.

Figure 3 shows the thickness PDDF and electron density profile for the illite. The PDDF suggests that the illite layers have an homogeneous electron distribution in contrast to bulk solution or water. The best calculated electron density from experimental data is positive from the symmetric center against water in bulk solution, and the overall profile has a good approximation of the theoretical profile of a smooth-sur-

https://doi.org/10.1346/CCMN.2001.0490401 Published online by Cambridge University Press

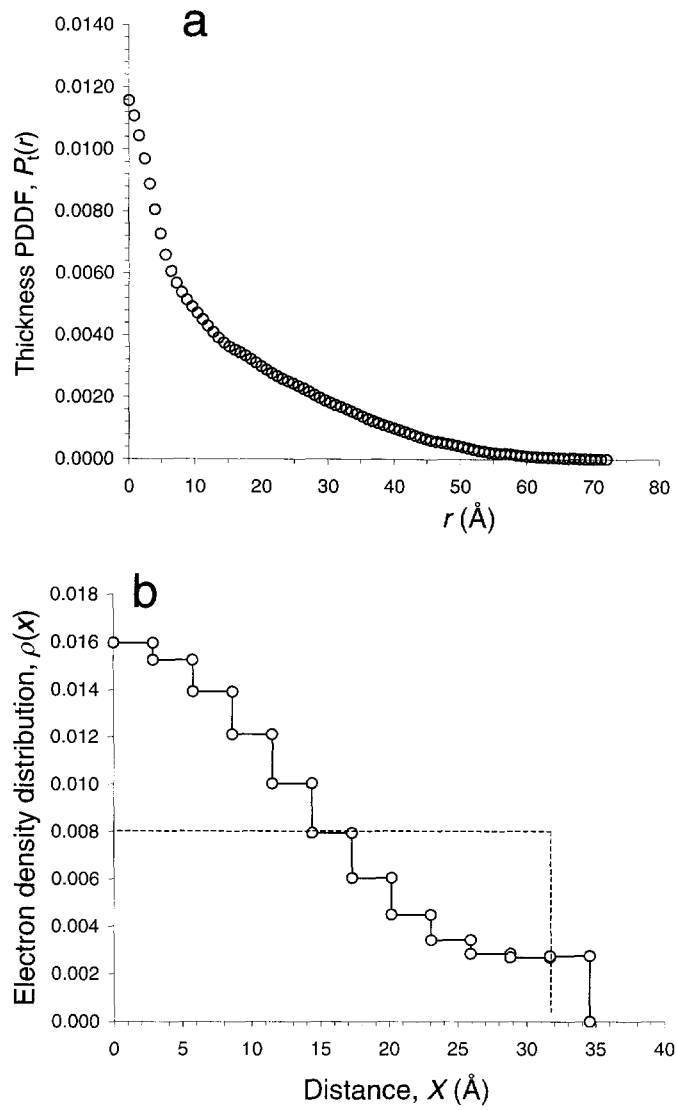


Figure 3. Thickness PDDF (a) and electron density profile (b) of illite in 2% particle suspension. The calculated electron density profile is based on a multi-step model; a theoretical representation of the profile for an illite particle with a smooth surface is depicted as a one-step function.

face illite layer (Figure 3b). The average thickness of this illite clay estimated from the two plots is ~6.5 nm. According to Hower and Mowatt (1966), the <0.5 μm fraction of this illite clay contains <15% smectite layers and has a CEC of 15 $cmol_c\ kg^{-1}$. The CEC of this illite sample (<0.1 μm) is 18 $cmol_c\ kg^{-1}$ as estimated by cationic surfactant adsorption. The thickness of illites measured by XRD peak broadening, TEM and fixed cation content may vary from a few to 100 nm depending on the percentage of smectite in the sample (Nadeau *et al.*, 1984; Środoń *et al.*, 1990, 1992; Drits *et al.*, 1997, 1998). Based on the percent smectite of the studied illite, the thickness (6–7 nm) determined by SAXS falls closely within the thickness range reported in those studies. Beckett *et al.* (1997) used sedimentation field-flow fractionation to determine the thickness of kaolinite and illite clays, and the plate thickness of one illite clay they determined was 5 to 10 times greater than that reported for the same sample by Drits *et al.* (1998). Note that the PDDF is curvilinear (Figure 3a), deviating from the shape expected for an ideal thin layer particle (Figure 1a). In addition, the electron density curve does not converge to zero at the maximum thickness (Figure 3b). This may indicate an underestimation of the thickness by this method. The greater thickness of particles makes them more prism-like to the X-ray beam so that longer lengths for the other two dimensions are required to treat the particles

https://doi.org/10.1346/CCMN.2001.0490401 Published online by Cambridge University Press

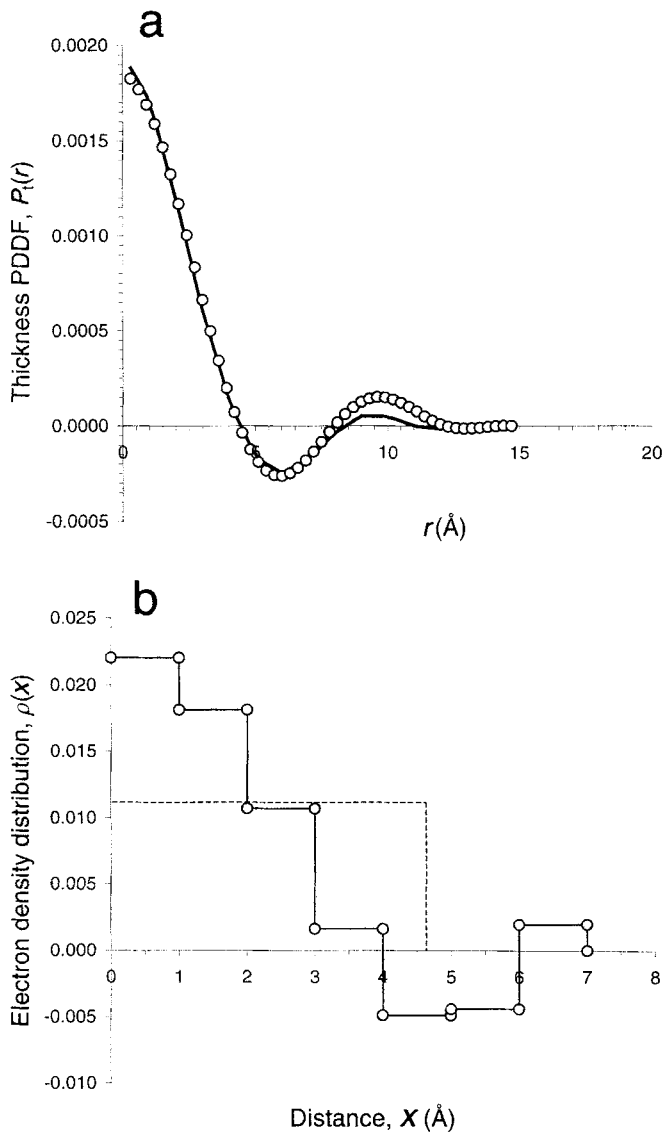


Figure 4. Thickness PDDF (a) and electron density profile (b) of montmorillonite in 0.5% suspension. A theoretical representation of the electron density profile for a montmorillonite layer with a smooth surface is depicted as a one-step function. The calculated electron density profile, based on a multi-step model, is used to fit the experimental PDDF (solid line as the best fit).

as lamellae. But the detection length of large dimensions is limited by the characterization length scale associated with the SAXS data used (~30 nm in this study). Therefore, the resolution for the thickness determination by SAXS is limited and estimated to be 7 to 8 nm. Thus, the thickness estimated in this study is close to the maximum allowed by the resolution of the method. A log-log plot of intensity ($I(q)$) *vs.* $q$ for this mineral (not shown) does show a $q^{-4}$ decay at high $q$, indicating a deviation from a thin-layer scattering which should show a $q^{-2}$ decay (as in the case of montmorillonite). Another possible factor causing the irregular PDDF curve is the polydispersity of particles as revealed in both the TEM (Środoń *et al.*, 1992) and the Guinier plot, in which the scattering intensity from particle thickness increases as $q$ approaches zero (not shown). The particle polydispersity might be reduced or eliminated by narrowing the particle size range of clay fractions during particle fractionation using centrifugation. The SAXS method is promising in this application because other methods used for measuring the thickness of fundamental particles of illites suffer difficulties such as swelling of smectite layers (XRD), stacking faults, and poor particle sampling (TEM).

https://doi.org/10.1346/CCMN.2001.0490401 Published online by Cambridge University Press

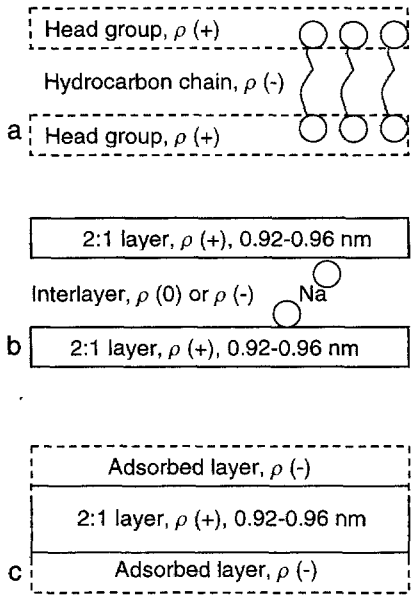


Figure 5. Possible schematic models for montmorillonite in dilute suspensions: cationic surfactant bilayer (a); two-layer montmorillonite particle (b); and a single montmorillonite layer with two distinct electron density regions (c). $\rho = \rho_{particle} - \rho_{water}$.

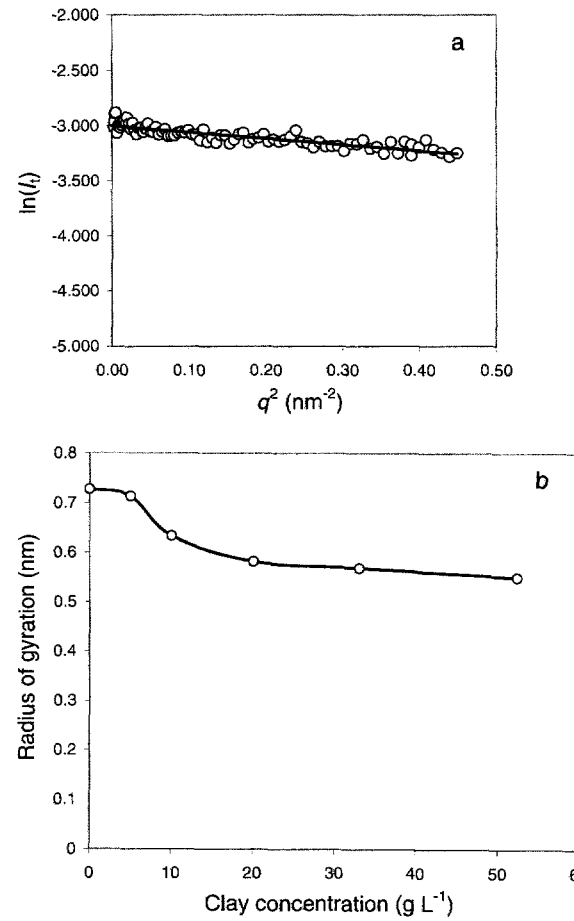


Figure 6. Thickness Guinier plot of the scattering curve of 0.5% montmorillonite suspension (a), and the relationship between the radius of gyration for thickness and the clay concentration (b).

Particles in SAXS samples, however, are dispersed and independent, and millions of particles are present in the scanned volume.

The PDDF and the electron density profile of montmorillonite are given in Figure 4. There are several characteristics of these plots that should be noted. (1) The PDDF oscillates when approaching zero, suggesting an inhomogeneous distribution of electrons in the montmorillonite layers (Figure 4a). (2) The PDDF approaches zero at 1.2 nm rather than at 0.92 nm as would be expected for a single 2:1 layer thickness (Figure 4a). This can be explained by the concept of effective thickness. The SAXS scattering intensity is dependent on the electron contrast between solvent and particles. Adsorbed Na cations and the hydration shell ought to result in an electron contrast with bulk water molecules. Thus, SAXS measures the thickness of Na-saturated montmorillonite layers up to somewhere in the first adsorbed cation layer. This thickness includes the 2:1 layer, adsorbed cations and hydration shell, and is presumably greater than the theoretical thickness of a single 2:1 layer. (3) The electron density profile (a multiple-step model) calculated from PDDF by deconvolution does predict a positive electron contrast from the midpoint of the 2:1 layer and outward (Figure 4b). (4) There exists a zone of negative electron contrast, measuring up to 0.15 nm on each side of the clay layer (Figure 4b).

Possible explanations for characteristics 1, 3 and 4 in Figure 4 lie in the schematic models for possible scatterers present in the system (Figure 5). Case 'a' is a self-organized cationic surfactant bilayer in which the hydrocarbon chain with a negative electron contrast is sandwiched by two layers of ordered ionic head groups with positive electron contrast. The scattering of such bilayers produces a PDDF depicted in Figure 1b (Iampietro *et al.*, 1998), with the same shape as that for montmorillonite (Figure 4a). But the PDDF, unlike the one for montmorillonite, predicts the full thickness of the bilayer, and the electron density profile takes a negative value at the profile's midpoint and becomes positive in the head group region (Iampietro *et al.*, 1998). Case 'b' depicts a layered montmorillonite arrangement with the presence of interlayer hydrated cations. This structure would give a PDDF like that obtained experimentally (Figure 4a). The difficulty with this model is that the experimental PDDF predicts a single-layer thickness rather than a two-layer thickness as in the case of the surfactant bilayer. This model also does not explain the negative dip in the experimental electron density profile shown in Fig-

https://doi.org/10.1346/CCMN.2001.0490401 Published online by Cambridge University Press

ure 4b. In case 'c', a single layer acts as an independent particle and this particle has two distinct electron density regions with the lower electron density region located at each interface. This model explains the particle thickness predicted by the PDDF and the patterns of the PDDF and the electron density profile. But we have to assume that the electron density in the interface is lower than that of the bulk solution resulting in a negative electron contrast. It is conceivable, however, that there exists a negative electron contrast at interfaces because the density of adsorbed water molecules has been found to be lower than that of free water at higher water contents (Martin, 1962).

Figure 6 shows the Guinier plot of the 0.5% scattering curve and the relationship between the derived radius of gyration for thickness and the clay concentration. The Guinier plot of montmorillonite scattering is typical for a thin-layer particle, *i.e.* a straight line of the plot of $\ln(I_t)$ *vs.* $q^2$ (Figure 6a). The concentration effect on the radius of gyration is most significant over the 0.5% to 2% clay concentration range, and is almost linear (Figure 6b). When the clay concentration is >2%, the concentration effect may reflect a reorganization of particles as indicated by a hump on scattering curves (Figure 2b). This invalidates the calculation of thickness from a Guinier plot and the radius of gyration. The 0.5% clay suspension and the extrapolated zero concentration produced almost the same radius of gyration indicating a minimum concentration effect. The corresponding particle thickness is 2.5 nm. This is the thickness of a two-layer montmorillonite particle with a two-layer water interlayer. Note that due to the resolution of the method, the thickness derived from the Guinier plot may contain up to 10% error. The result seems to support the model of case 'b' in Figure 5. However, this interlayer configuration should result in a positive electron density contrast because of a greater water density (Martin, 1962). Furthermore, if montmorillonite particles act as in case 'c', due to the electron inhomogeneity, the radius of gyration from a Guinier plot cannot be used for thickness calculation (Glatter, 1991). This question is currently under investigation.

## CONCLUSIONS

The indirect Fourier transform of small-angle X-ray scattering data has been used to determine the thickness and surface properties of two common clay minerals. For an illite system, the PDDF gave a correct description of particle geometry, and the calculated electron density profile is in accordance with the theoretical electron density distribution for this mineral. This study demonstrates the possibility that the thickness of fundamental particles of illites can be determined while avoiding the difficulties encountered in other methods. Both the PDDF and the electron density profile accurately predict the thickness of Na-montmorillonite layers, and the results suggest that there exists an electron inhomogeneity at the interface of this mineral. The models for possible scatterers present in dilute montmorillonite suspensions are proposed and discussed.

## ACKNOWLEDGMENTS

The project is supported by a grant from the USDA National Research Initiative Competitive Grants program through award number 98-35107-6515. The research at Oak Ridge was sponsored in part by the US Department of Energy under Contract No. DE-AC05-00OR22725 with the Oak Ridge National Laboratory, managed by the UT-Battelle, LLC.

## REFERENCES

Beckett, R., Murphy, D., Tadjiki, S., Chittleborough, D.J. and Giddings, J.C. (1997) Determination of thickness, aspect ratio and size distributions for platy particles using sedimentation field-flow fractionation and electron microscopy. *Colloids and Surfaces,* **120,** 17–26.

Drits, V.A., Środoń, J. and Eberl, D.D. (1997) XRD measurement of mean thickness of illite/smectite; reappraisal of the Kübler index and the Scherrer equation. *Clays and Clay Minerals,* **45,** 461–475.

Drits, V.A., Eberl, D.D. and Środoń, J. (1998) XRD measurement of mean thickness, thickness distribution and strain for illite and illite-smectite crystallites by the Bertaut-Warren-Averbach technique. *Clays and Clay Minerals,* **46,** 38–50.

Glatter, O. (1977) Data evaluation in small angle scattering: calculation of the radial electron density distribution by means of indirect Fourier transformation. *Acta Physica Austriaca,* **47,** 83–102.

Glatter, O. (1980) Determination of particle-size distribution functions from small-angle scattering data by means of the indirect transformation method. *Journal of Applied Crystallography,* **13,** 7–11.

Glatter, O. (1982) Data treatment and Interpretation. Pp. 119–196 in: *Small-Angle X-Ray Scattering* (O. Glatter and O. Kratky, editors). Academic Press, New York.

Glatter, O. (1991) Scattering studies on colloids of biological interest (amphiphilic systems). *Progress in Colloid and Polymer Science,* **84,** 46–54.

Glatter, O. (1995) Modern methods of data analysis in small-angle scattering and light scattering. Pp. 107–180 in: *Modern Aspects of Small-Angle Scattering* (H. Brumberger, editor). Proceedings of the NATO Advanced Study Institutes, Como, Italy, May 1993. Kluwer Academic Publishers, Dordrecht, The Netherlands.

Glatter, O., Strey, R., Schubert, K.V. and Kaler, E.W. (1996) Small angle scattering applied to microemulsions. *Berichte. Bunsengesellschaft fuer Physkalische Chemie,* **100,** 323–335.

Guinier, A. and Fournet, G. (1955) *Small Angle Scattering of X-rays.* J. Wiley & Sons, New York, 268 pp.

Hight, R.J. Jr., Higdon, W.T. and Schmidt, P.W. (1960) Small angle X-ray scattering study of sodium montmonrillonite clay suspensions. *Journal of Chemical Physics,* **33,** 1656–1661.

Hight, R.J. Jr., Higdon, W.T., Darley, H.C. and Schmidt, P.W. (1962) Small angle x-ray scattering from montmorillonite clay suspensions. II. *Journal of Chemical Physics,* **37,** 502–510.

Hower, J. and Mowatt, T.C. (1966) The mineralogy of illites and mixed-layer illite/montmorillonites. *American Mineralogist,* **51,** 825–855.

Iampietro, D.J., Brasher, L.L., Kaler, E.W., Stradner, A. and Glatter, O. (1998) Direct analysis of SANS and SAXS measurements of cationic surfactant mixtures by Fourier transformation. *Journal of Physical Chemistry B,* **102,** 3105–3113.

Martin, R.T. (1962) Adsorbed water on clay: a review. *Clays and Clay Minerals,* **9,** 28–70.

Morvan, M., Espinat, D., Lambard, J. and Zemb, Th. (1994) Ultrasmall- and small-angle X-ray scattering of smectite clay suspensions. *Colloids and Surfaces A,* **82,** 193–203.

Müller, K. and Glatter, O. (1982) Practical aspects to the use of indirect Fourier transformation methods. *Makromolekulare Chemie,* **183,** 465–479.

Nadeau, P.H., Wilson, M.J., McHardy, W.J. and Tait, J.M. (1984) Interstratified clays as fundamental particles. *Science,* **225,** 923–925.

Pignon, F., Magnin, A., Piau, J.M., Cabane, B., Lindner, P. and Diat, O. (1997) Yield stress thixotropic clay suspension: Investigations of structure by light, neutron, and X-ray scattering. *Physical Review E,* **56,** 3281–3289.

Pilz, I. (1982) Proteins. Pp. 239–293 in: *Small-Angle X-ray Scattering* (O. Glatter and O. Kratky, editors). Academic Press, New York.

Porod, G. (1982) General theory. Pp. 17–51 in: *Small-Angle X-ray Scattering* (O. Glatter and O. Kratky, editors). Academic Press, New York.

Rich, C.I. and Barnhisel, R.I. (1977) Preparation of clay samples for X-ray diffraction analysis. Pp. 797–808 in: *Minerals in Soil Environments* (J.B. Dixon and S.B. Weed, editors). Soil Science Society of America, Madison, Wisconsin.

Saunders, J.M, Goodwin, J.W., Richardson, R.M. and Vincent, B. (1999) A small-angle X-ray scattering study of the structure of aqueous Laponite dispersions. *Journal of Physical Chemistry B,* **103,** 9211–9218.

Schmidt, P.W. (1995) Some fundamental concepts and techniques useful in small-angle scattering studies of disordered solids. Pp. 1–56 in: *Modern Aspects of Small-Angle Scattering* (H. Brumberger, editor). Proceedings of the NATO Advanced Study Institutes, Como, Italy, May 1993, Kluwer Academic Publishers, Dordrecht, The Netherlands.

Środoń, J., Andreolli, C., Elsass, F. and Robert, M. (1990) Direct high-resolution transmission electron microscopic measurement of expandability of mixed-layer illite/smectite in bentonite rock. *Clays and Clay Minerals,* **38,** 373–379.

Środoń, J., Elsass, F., McHardy, W.J. and Morgan, D.J. (1992) Chemistry of illite-smectite inferred from TEM measurements of fundamental particles. *Clay Minerals,* **27,** 137–158.

Strey, R., Glatter, O., Schubert, K.V. and Kaler, E.W. (1996) Small-angle neutron scattering of $D_2O$-$C_{12}E_5$ mixtures and microemulsions with n-octane: Direct analysis by Fourier transformation. *Journal of Chemical Physics,* **105,** 1175–1188.

Taylor, T.R. and Schmidt, P.W. (1969) Interparticle potential energies in Na-montmorillonite clay suspensions. *Clays and Clay Minerals,* **17,** 77–82.

van Olphen, H. (1963) *An Introduction to Clay Colloid Chemistry.* John Wiley & Sons, New York, 301 pp.

van Olphen, H. and Fripiat, J.J. (1979) *Data Handbook for Clay Materials and Non-metallic Minerals.* Pergamon, Oxford, UK, 346 pp.

Wignall, G.D., Lin, J.S. and Spooner, S. (1990) The reduction of parasitic scattering in small-angle X-ray scattering by three pinhole collimating system. *Journal of Applied Crystallography,* **23,** 241–246.

E-mail of corresponding author: James_Rice@sdstate.edu

*(Received 7 October 2000; revised 5 March 2001; Ms. 492; A.E. Peter J Heaney)*